Key Points:
- The density of the very slow solar wind drops significantly in Cycle 24
- The source properties of the rarefied very slow solar wind are determined

Correspondence to:
M. Tokumaru,
tokumaru@isee.nagoya-u.ac.jp

Rarefaction of the Very Slow (<350 km/s) Solar Wind in Cycle 24 Compared With Cycle 23

Munetoshi Tokumaru[1] [ID], **Tomoya Shimoyama[1]**, **Ken'ichi Fujiki[1]** [ID], **and Kazuyuki Hakamada[2]** [ID]

[1]Institute for Space-Earth Environmental Research, Nagoya University, Nagoya, Japan, [2]Department of Natural Science and Mathematics, Chubu University, Kasugai, Japan

Abstract We investigate long-term variation of the very slow solar wind (VSSW), whose speed is less than 350 km/s, during the period between 1997 and 2015, that is, Cycles 23 and 24, using interplanetary scintillation measurements, which enable determination of the global distribution of the flow speed and the electron density fluctuation level ΔN_e. We find that the occurrence rate of VSSW increases in the maximum phase of the solar cycle, and it was mostly associated with high ΔN_e in Cycle 23. However, the VSSW is found to be more associated with low ΔN_e in Cycle 24. This fact is consistent with an increased occurrence of the low-density VSSW observed in situ in Cycle 24. These facts, which are considered to be a manifestation of weak solar activity in this cycle, suggest that the VSSW has become significantly rarefied in recent years. We identify the source region of the VSSW on the photosphere using a potential field analysis and examine the magnetic field properties of the VSSW source. We find that the low-ΔN_e VSSW is associated with a smaller expansion factor and possibly a slightly weaker photospheric field strength than the high-ΔN_e VSSW. The results obtained here may suggest that more open magnetic field areas producing the VSSW in Cycle 24 are formed in the quiet Sun region, which is associated with a lower mass flux supply into the corona, than those in Cycle 23.

1. Introduction

The fast (700–800 km/s) and slow (300–400 km/s) solar wind are known to be associated with rarefied and dense plasma, respectively. The typical density at 1 AU is $1-7/cm^3$ for the fast wind and $7-15/cm^3$ for the slow wind (Russell et al., 2016). The cause for this inverse relation between speed and density is not fully understood, but this fact may suggest the constancy of physical parameters of the solar wind such as mass, momentum, and energy fluxes among different flow tubes (Le Chat et al., 2012; Mullan, 1983; Neugebauer, 1992; Richardson & Wang, 1999; Steinitz & Eyni, 1980). A similar inverse relation is found between solar wind speed and density fluctuations, ΔN_e, derived from interplanetary scintillation (IPS) measurements; that is, the fast (slow) wind is associated with low (high) ΔN_e (Asai et al., 1998; Tokumaru et al., 2012). The ΔN_e observed by IPS represents the level of microturbulence with a scale size smaller than 10^3 km in the solar wind and serves as a proxy of the solar wind density N; that is, $N \propto \Delta N_e$ to a first-order approximation (Coles et al., 1978). The empirical relation $\Delta N_e \propto V^{-0.5\pm0.15}$, where V is the solar wind speed, was deduced from an earlier study using IPS observations in 1995 (Asai et al., 1998). This result was confirmed by a subsequent study using IPS observations during 1997–2009: a similar index of the best fit power law function was derived: $\Delta N_e \propto V^{-0.36\pm0.14}$ for $V > 350$ km/s (Tokumaru et al., 2012). These empirical formulas are basically consistent with the inverse relation between V and N, while they are considered to include the effect of a radial evolution of microturbulence in the solar wind (Asai et al., 1998).

The subsequent study also revealed that there is a break in the inverse relation between V and ΔN_e at $V < 350$ km/s (Tokumaru et al., 2012). Figure 1 shows the V versus ΔN_e plots derived from IPS observations in (a, b) 1998 and (c, d) 2009. Figures 1a and 1c are adopted from Figure 11 of Tokumaru et al. (2012), and they show the relation between V and ΔN_e in the linear-linear format. Figures 1b and 1d are basically the same as Figures 1a and 1c, but they show the data in the 2-D map with a log-log scale. Here ΔN_e is given by a relative value normalized by the mean level of the slow solar wind. The regression line determined for $V > 350$ km/s is indicated by a solid line in each plot. We note that the regression lines in Figures 1a and 1c are linear fits, whereas those in Figures 1b and 1d are log-log (i.e., power law) fits. The IPS data for 1998 show a fairly good match with the regression line for the entire range of V including $V < 350$ km/s in spite of large
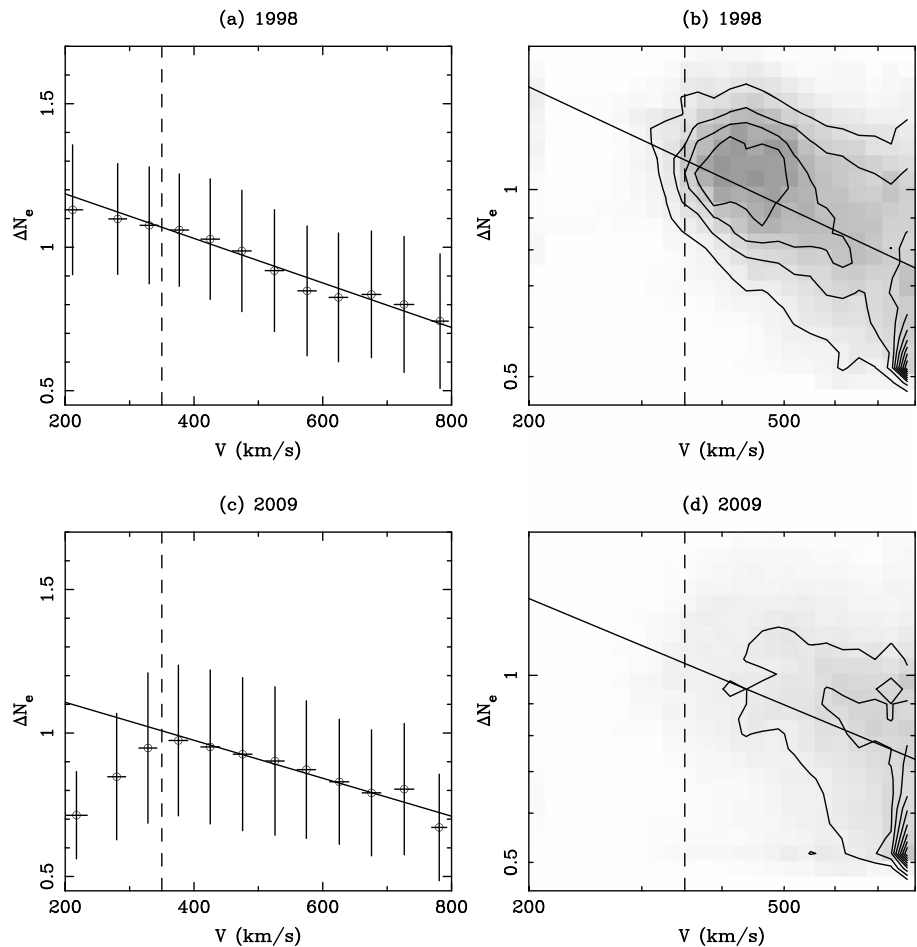
Figure 1. Relation between V and ΔN_e for (a, b) 1998 and (c, d) 2009. Plots (a) and (c) are presented in the linear-linear format. Vertical and horizontal bars indicate root-mean-square deviations of the mean for ΔN_e and V for each bin. In plots (b) and (d), the occurrence frequency is plotted in a 2-D map with a log-log scale by solid contour lines and gray shades. The oblique solid line in each plot is either (a, c) the best fit linear function or (b, d) the best fit power law function for $V > 350$ km/s (indicated by dashed line).

root-mean-square (rms) deviations on the mean. Those for 2009, however, show a significant discrepancy between the regression line and IPS observations for $V < 350$ km/s. This fact indicates that this low-speed wind is associated with low ΔN_e. The level of ΔN_e for 200–300 km/s is ∼0.7, nearly the same as that for the fast (700–800 km/s) wind. Thus, our IPS data for 2009 suggest that the density of such a slow solar wind is as low as that of the fast wind. No detailed survey on this finding has been made until the present study.

The solar wind with $V < 350$ km/s wind is classified as the very slow solar wind (VSSW) and is known to have different properties from those of the ordinary slow wind with $V > 350$ km/s (Kojima et al., 1999; Ohmi et al., 2004; Sanchez-Diaz et al., 2016). IPS observations showed that the VSSW originates from a compact area on the photosphere associated with rapidly diverging open-field lines rooted in the vicinity of the active region (Kojima et al., 1999; Ohmi et al., 2004). This fact is consistent with the inverse relation between the solar wind speed and the flux expansion factor (Hakamada & Kojima, 1999; Wang & Sheeley, 1990). The in situ properties of the VSSW were investigated using observations made by two Helios spacecraft (Sanchez-Diaz et al., 2016). The VSSW was found to have higher density, lower temperature, and lower helium abundance than the regular slow wind, and this result is qualitatively consistent with a continuation of the regular slow wind. However, the properties of the VSSW determined from Helios observations appear inconsistent with the drop in ΔN_e found from our IPS observations for $V < 350$ km/s.

In the present study, we focus on a break in the V-ΔN_e relation at $V < 350$ km/s and the properties of the VSSW associated with low ΔN_e in detail. The outline of this paper is as follows. In section 2, we describe our IPS observations and other data used in this study. This study spans the period from 1997 to 2015, corresponding

to that from near the Cycle 23 minimum to the Cycle 24 declining phase. In section 3, we present the long-term change in the VSSW and its dependence on ΔN_e during the analysis period. In section 4, we compare our IPS data with in situ measurements of the VSSW. In section 5, we present properties of the source region for the low-ΔN_e VSSW using calculations of a potential field source surface (PFSS) model. In sections 6 and 7, we discuss and summarize and discuss the results obtained here.

2. Observations

2.1. ISEE IPS Observations

IPS observations have been regularly conducted since the 1980s at the Institute for Space-Earth Environmental Research (ISEE; formerly Solar-Terrestrial Environment Laboratory) of Nagoya University using the 327-MHz multistation system (Kojima & Kakinuma, 1990; Tokumaru, 2013). The solar wind speeds are derived from the cross-correlation analysis of multistation IPS data. Since 1997, the scintillation disturbance factor, the g value, which represents the relative change in the integrated level of ΔN_e along the line of sight (LOS), has also been derived from ISEE IPS observations (Tokumaru et al., 2000). ISEE IPS data are available from our ftp server (ftp://ftp.isee.nagoya-u.ac.jp/pub/vlist). Here it should be noted that the speed and g value data are the integration of the weighted actual parameters (speed or ΔN_e) along the LOS. The LOS integration sometimes affects IPS observations significantly, and hence, a deconvolution analysis of IPS observations is needed to obtain accurate estimates of the speed and ΔN_e. In this study, we employed the time-sequence tomography method, which enables us to retrieve the quasi-stationary structure of the solar wind from IPS observations (Fujiki et al., 2003; Kojima et al., 2007). The method used here is the same as the one used in our earlier studies (Tokumaru et al., 2012, 2015). In this analysis, the speed and g value data are deconvolved simultaneously by assuming weak scattering and a constant-speed radial flow beyond the source surface at 2.5 $R_\odot$. We performed the tomographic analysis of our IPS observations during 1997–2015 on a yearly basis. Note that IPS data for 2010 are unavailable owing to the observation system upgrade. Because our IPS observations are interrupted in winter owing to snow, the deconvolved data for a given year usually cover a period of 10 or 11 solar rotations. In addition, interruption of IPS observations occurs due to irregular system maintenance, and the coverage varies with years. This variation in the observation coverage is corrected, as will be described below. Therefore, we consider that it does not significantly bias the results of the present study.

Figures 2a and 2b show the synoptic source surface maps of the solar wind speed and ΔN_e, respectively, derived from the tomographic analysis of our IPS observations for Carrington rotation 1927, which corresponds to the period 7 September to 4 October 1997. The color in these maps represents either the speed or ΔN_e, and the black broken line in each map indicates the magnetic neutral line, which was calculated from photospheric field observations at Wilcox Solar Observatory with a PFSS model (http://wso.stanford.edu/synsourcel.html). The speed map (Figure 2a) clearly shows the bimodal structure of the solar wind, which is composed of the fast wind at latitudes higher than 30° and the slow wind at lower latitudes. This is a typical feature of the solar wind near the solar minimum (Kojima et al., 1998; Phillips et al., 1995). A similar bimodal feature is found in the ΔN_e map (Figure 2b); that is, the low- (high-) ΔN_e region is located at high (low) latitudes, and thus, an inverse relation between the speed and ΔN_e is revealed here. We note that the shape of the slow wind region does not exactly match that of the high-ΔN_e region, and the high-ΔN_e region has a more patchy distribution on the source surface than the slow wind region.

In this study, we determined the source surface area corresponding to $V < 350$ km/s. Thick solid lines in the figures indicate boundaries of the region with $V < 350$ km/s, hereafter, the VSSW region. As addressed in our earlier study (Kojima et al., 1999), the locations of the VSSW do not follow the magnetic neutral line owing to the effect of large flux expansion near active regions. We summed the area of the VSSW region on a yearly basis and divided it by the total area covered by our IPS observations in the given year to yield the fractional area. This normalization is to correct the different coverage of our IPS observations for each year.

2.2. In Situ Measurements

For comparison with our IPS observations in this study, we analyzed in situ data collected with the Solar Wind Electron Proton Alpha Monitor (McComas et al., 1998) on board the Advanced Composition Explorer (ACE) spacecraft. We used the hourly averaged Level 2 (verified) data adopted from the ACE Science Center (http://www.srl.caltech.edu/ACE/ASC/index.html). We note here that no ACE in situ data are available before 1998 and that ACE has some instrumental issues since 2010 (see http://www.srl.caltech.edu/ACE/ASC/ACE_repointing.pdf). Since the yearly averaged values were derived here from in situ measurements
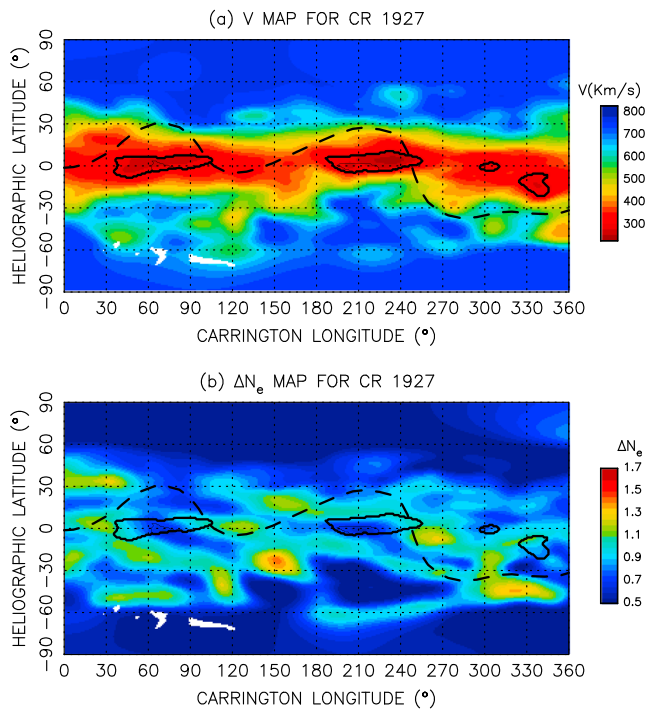
Figure 2. Synoptic source surface maps of (a) the solar wind speed V and (b) density fluctuations ΔN_e derived from Institute for Space-Earth Environmental Research interplanetary scintillation observations for Carrington rotation (CR) 1927 (7 September to 4 October 1997). Red (blue) colors represent slow (fast) speeds in (a) and high (low) ΔN_e in (b). Black solid lines indicate boundaries of the regions with $V < 350$ km/s; that is, the very slow solar wind. Dashed lines in each map indicate the magnetic neutral line on the source surface computed from magnetograph observations at Wilcox Solar Observatory (http://wso.stanford.edu/synsourcel.html).

to compare with the IPS data, the effect of the latitude variation of the ACE's location relative to the solar equator was ignored.

2.3. Magnetograph Observations

We analyzed magnetograph observations at Kitt Peak National Solar Observatory (http://nsokp.nso.edu/) using a model (Hakamada & Kojima, 1999) to investigate the magnetic field properties of the VSSW source region. The source surface is assumed to be located at 2.5 $R_\odot$ in this analysis. We determined the location of the VSSW source on the photosphere at 1 $R_\odot$ by tracing the field line of the potential field model from the source surface at 2.5 $R_\odot$ and then calculated the photospheric field strength $|B_P|$ and the flux expansion factor $f \equiv (B_P/B_{SS})(R_\odot/R_{SS})^2$, where B_{SS} and R_{SS} are the source surface field and the source surface distance, that is, 2.5 $R_\odot$. The data of $|B_P|$ and f were averaged on a yearly basis over the source surface area corresponding to given solar wind speed and ΔN_e ranges. We also used magnetograph observations at Wilcox Solar Observatory to determine the magnetic neutral line on the source surface, as mentioned above.

3. Long-Term Variations of VSSW and Dependence on ΔN_e

Figure 3a shows the yearly variation of the fractional areas of the VSSW during 1997–2015. The fractional areas of the VSSW range between ~15% and ~5% and systematically change with the solar cycle. They exhibit distinct peaks near the Cycle 23 and 24 maxima; 14.3% and 15.2% in 1999 and 2012, respectively, and they are minimal in the declining phase of Cycle 23, 4.4% and 4.7% in 2003 and 2005, respectively. Although the solar activity at the Cycle 24 maximum is much weaker than that at the Cycle 23 maximum, no significant difference between the VSSW fractional areas at Cycle 23 and 24 is found from the figure.

In this study, we sorted the VSSW data into five groups in terms of ΔN_e, as we did in our earlier study (Tokumaru et al., 2012). The values corresponding to the boundaries of the five g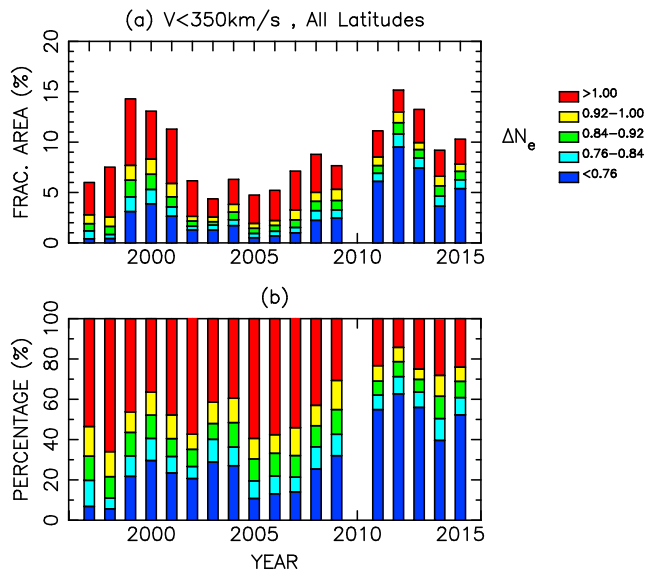roups are 0.76, 0.84, 0.92, and 1.0. (This set of boundary values is the same as that used in the earlier study.) The sorting results are indicated in Figure 3 by color. Figure 3b shows the yearly variation of a percentage of each ΔN_e range during 1997–2015. A striking feature revealed in this feature is a drastic growth (decay) of the VSSW associated with the lowest- (highest-) ΔN_e range during the analysis period, while modulation due to the solar cycle effect is still discernible from the figure. The VSSW observed in Cycle 23 was mostly associated with high ΔN_e (>1.0), and the percentage of the VSSW with $\Delta N_e < 0.76$ was 18% on average. By contrast, the VSSW associated with low ΔN_e (<0.76) increased to 46% in Cycle 24. Low- and high-Δ VSSW data show either a peak or a valley at around solar maxima: 2000 and 2012. According to the inverse relation between V and ΔN_e (see Figure 1), the level of $\Delta N_e < 0.76$ corresponds to the fast wind ($V > 700$ km/s), and our IPS data suggest that more than 50% of the VSSW observed after 2011 is associated with ΔN_e as low as the fast wind level. However, the solar cycle effect is overwhelmed by a monotonic change in the low- and high-ΔN_e VSSW. Here it should be noted that the percentage of the low-ΔN_e VSSW basically increases at around solar maxima and decreases at the periods near solar minima: 1998 and 2005, and that it also increases in the declining phase: 2003 and 2004. Another interesting point to note is that the percentage of the VSSW associated with the intermediate range of ΔN_e is almost constant over the analysis period. Thus, a marked change occurs only for high (>1.0) and low (<0.76) levels of ΔN_e.

For comparison, we examine IPS data for the fast solar wind ($V > 700$ km/s). Figure 4 shows the time variations of (a) fractional areas and (b) percentages of different ΔN_e ranges for $V > 700$ km/s during 1997–2015. The fractional areas of the fast wind (Figure 4a) show a clear dependence on the solar cycle, but a peak of fast wind data occurs at the solar minimum, that is, 2007. Furthermore, the low-ΔN_e (<0.76) group is always dominant in the fast wind data throughout the period except for 2000, and the effect of the solar cycle is hardly observed in the percentage data of the fast wind (Figure 4b). An increasing trend for the low-ΔN_e group

Figure 3. Yearly variations of (a) the source surface fractional area of very slow solar wind and (b) the percentages of very slow solar wind areas corresponding to 5 ΔN_e ranges: (red) >1, (yellow) 1–0.92, (green) 0.92–0.84, (cyan) 0.84–0.76, and (blue) < 0.76 for all latitudes.

appears to be present in the fast wind data: however, the trend is less prominent than in the case of the VSSW. The deficit of the low-ΔN_e group for 2000 is considered due to the blurring effect of spatial resolution of the IPS tomography caused by rapid variation of the solar wind structure at the solar maximum (see Kojima et al., 2004).

Next, we examine the VSSW data at low latitudes for comparison with the in situ data taken with the ACE spacecraft (see the next section). Here one should keep in mind that the IPS observations provide global information on the solar wind, whereas the ACE in situ measurements represent the solar wind in the ecliptic plane, that is, near the solar equator. Figure 5 demonstrates the VSSW data for low latitudes, within 10° around the equator. The fractional areas of the VSSW for low latitudes are somewhat larger than those for all latitudes, mostly ranging between ~10% and ~25%. This fact is ascribed to a higher occurrence rate of the VSSW at low latitudes than other latitudes, since the denominator to derive the factional area data shown in Figure 5a is given by the total area covered by IPS observations for low latitudes. The time variations of the percentage for high- and low-ΔN_e VSSW at low latitudes are similar to those for all latitudes, but they appear to be less distinct. This is partly due to a smaller number of data. The low-ΔN_e VSSW is not a majority in the low-latitude data at the Cycle 24 maximum unlike the data for all latitude, and also, that peaks and valleys of the VSSW fractional area data occur in different years: 1997 and 2008 (see Figure 5a). These differences may be due to an intrinsic effect related to the latitude dependence of the VSSW distribution rather than an effect of insufficient statistics. Nevertheless, the IPS data at low latitudes clearly demonstrate long-term trends for the rise and decline of the low- and high-ΔN_e VSSWs, respectively. The percentages of the low-ΔN_e VSSW for low latitudes show peaks in 2000 and 2012, which are the same as the ones in all latitudes (see Figure 5b).

4. Comparison With In Situ Measurements

Figure 6 shows 2-D histograms of the solar wind speed V and density N measured by ACE/Solar Wind Electron Proton Alpha Monitor for (a) 1998 and (b) 2009. The inverse relation between V and N is clearly observed in these plots, similar to the IPS data shown in Figure 1. We selected the data with $V < 350$ km/s (vertical dashed line in the figure) as the VSSW. We then sorted the VSSW data in terms of N into two groups: that is, low- and high-density VSSWs. The value of $5/cm^3$ (horizontal dashed line in the figure) is used as a threshold density. This value is selected to be well below the typical density of the ordinary slow solar wind. Here we should note that the in situ data taken at 1 AU contain the effect of stream-stream interaction during propagation. This effect can be significant particularly for the VSSW (Sanchez-Diaz et al., 2016).
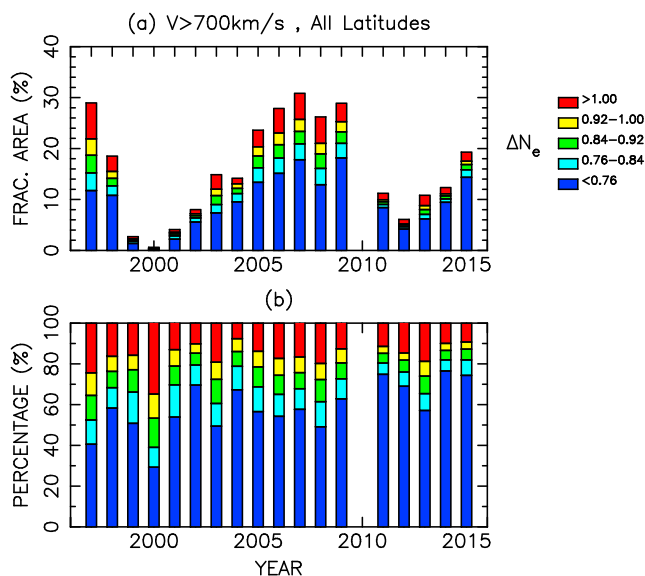
Figure 7a indicates the yearly variation in the occurrence rate calculated for all the VSSW (red bars) and the low-density VSSW (blue bars). The occurrence rate is given by the ratio of the number of data to that of all data observed for a given year. The occurrence rates of the VSSW vary with the solar cycle, ranging from <1% in 2003 to ~16% in 1998. We note that the occurrence rates of the VSSW data show a valley in the period just before the solar minimum, that is, the declining phase of Cycle 23 and a peak at the ascending phase of Cycle 23. The occurrence rates of the low-density VSSW also show a similar dependence on the solar cycle, but the peak at Cycle 23 is significantly weaker than that at Cycle 24. In the case of all the VSSW data (red), the peak level for 2012 is nearly the same as that for 1998. Another important point revealed in the figure is that a systematic increase dominates the time variation of the low-density VSSW occurrence. This fact is clearly discernible in Figure 7b, which shows the percentage
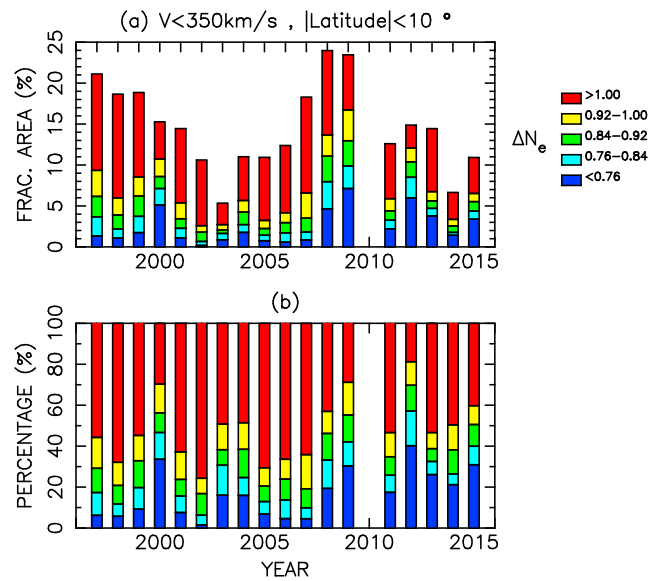

Figure 4. The same as Figure 3 but for fast (>700 km/s) winds.

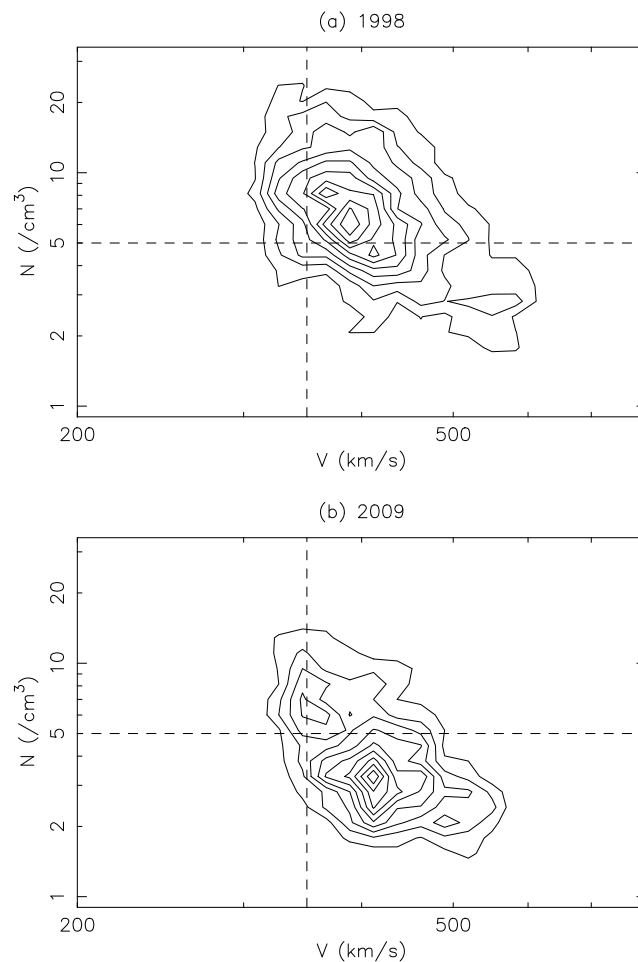**Figure 5.** The same as Figure 3 but for low (< 10°) latitudes.

Figure 6. Relation between V and N measured in situ for (a) 1998 and (b) 2009. The occurrence frequency is plotted in a 2-D map by contour lines. Vertical and horizontal dashed lines correspond to $V = 350$ km/s and $N = 5$ /cm^3, respectively.
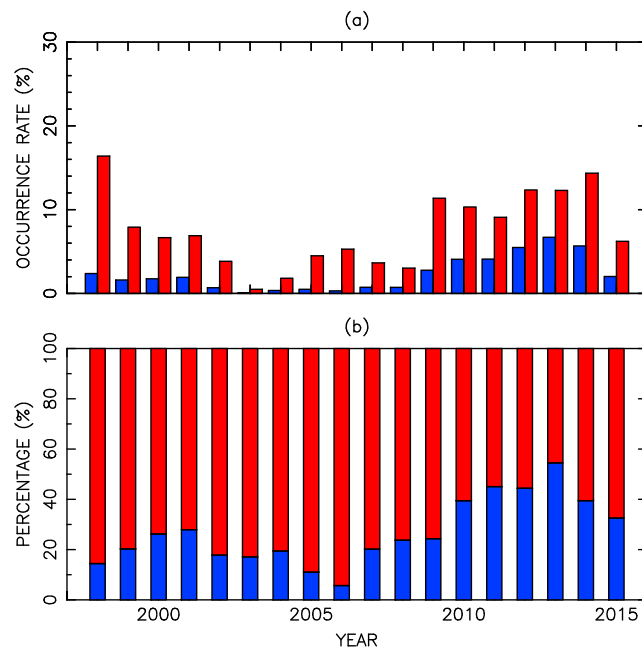
Figure 7. Yearly variation of (a) occurrence rates and (b) percentages of very slow solar wind associated with (red) $N > 5/cm^3$ and (blue) $N < 5/cm^3$.

of the VSSW associated with either low or high density. More than 80% of the VSSW is associated with high density ($>5/cm^3$) in 1998, and the percentage of the high-density VSSW grows to more than 90% in 2006 (the late declining phase of Cycle 23), after a slight decline at the Cycle 23 maximum. The high-density VSSW continues to decline after the Cycle 23/24 minimum, and its occurrence rate becomes minimum ($\sim$48%) in 2013, that is, near the Cycle 24 maximum. Thus, the low-density VSSWs are observed more frequently at the solar maximum, particularly in Cycle 24. These features of VSSWs revealed from in situ measurements are consistent with those revealed from IPS observations, if $N \propto \Delta N_e$ (see Figure 3).

Figure 8 shows the comparison between in situ and IPS VSSW data for (a) all and (b) low ($\pm 10°$) latitudes. In these figures, yearly values of the occurrence rate of low-density ($<5/cm^3$) VSSW are plotted versus those of the low-ΔN_e (<0.76) VSSW factional area. A significant positive correlation between in situ and IPS data is revealed from each plot. The correlation coefficients are 0.90 and 0.64 for (a) all and (b) low latitudes, respectively. This result suggests that the long-term trend found for ΔN_e data represents that for the solar wind density. A poorer correlation between in situ and IPS data for low latitudes is mostly ascribed to insufficient statistics due to the reduced number of data. The number of the low-latitude data reduces to 18% of the all latitude data, and the fractional area of the VSSW is originally small: usually less than 15%. Hence, the statistics become significantly poor when the low-latitude data are used. Furthermore, the relation between N and ΔN_e may include more complicated processes than that assumed in the present study: that is, $N \propto \Delta N_e$. The error caused by this fact is considered to degrade the correlation under the condition of poor statistics. The result obtained here also implies that the effect of stream-stream interaction does not significantly influence in situ observations of the VSSW at 1 AU.

5. Properties of VSSW Source
5.1. Latitude Distribution of VSSW Source
We sorted the VSSW data derived from the IPS observations in terms of the heliographic latitude of the foot region on the photosphere into four groups (0–15°, 15–30°, 30–50°, and 50–90°). Figure 9 shows the IPS data sorted in terms of the latitude for (a, c) all VSSW ($V < 350$ km/s) and (b, d) low-ΔN_e VSSW ($V < 350$ km/s and $\Delta N_e < 0.76$). The upper panels (a, b) of the figure show the annual variations of the fractional areas, and the lower panels (c, d) show those of the percentage for the four latitude ranges. As shown here, most of the VSSW sources are located at latitudes less than 30° during the whole period except for a few year periods around solar minima. The averaged percentage for 0–30° is 67% for the whole period. The VSSW sources tend
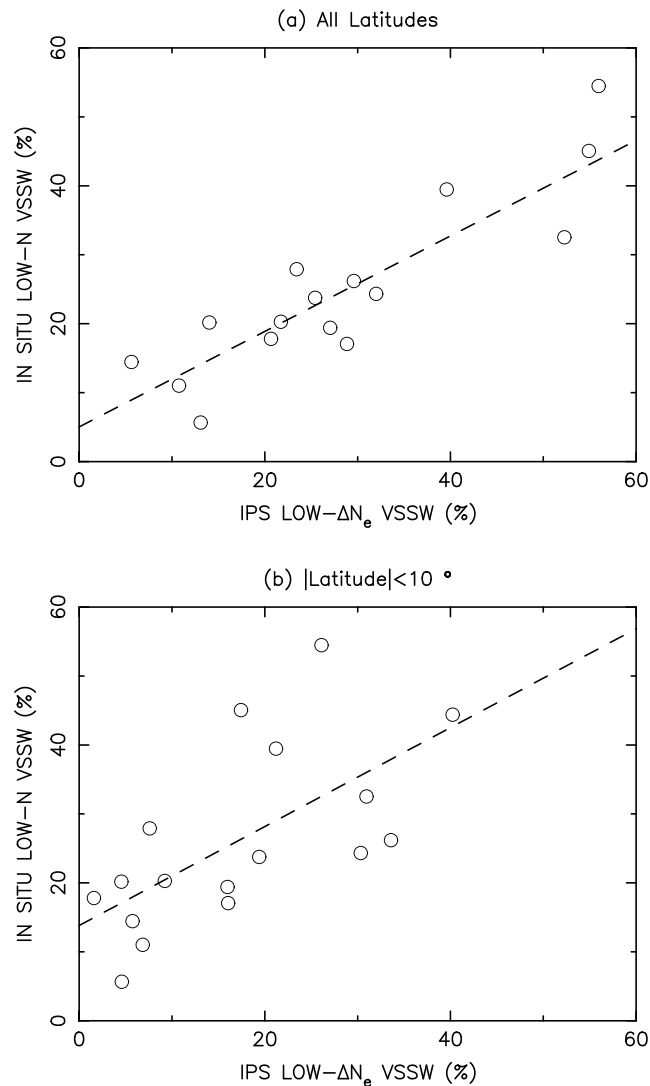
Figure 8. Correlation between low-ΔN_e very slow solar wind (VSSW) observed by IPS and low-density VSSW observed in situ for (a) all and (b) low (10°) latitudes. Dashed lines indicate least squares fitted linear functions. The correlation coefficients are 0.90 and 0.64 for (a) and (b), respectively. IPS = interplanetary scintillation.

to be located at lower latitudes (0–15°) in the late declining phase, and 61% of the VSSW sources were located at 0–15° in 2006. This fact is considered to be closely linked with the solar cycle variation of the sunspot latitude, since the VSSW was found to originate from a compact open-field region near the active region (Kojima et al., 1999; Ohmi et al., 2004). High-latitude (50–90°) VSSW sources increase in 1997 and 2008: near or at the solar minimum. This fact may be related to the fact that the open-field regions tend to occur at high latitudes at the solar minimum. These open-field regions, that is, the coronal holes, are mostly associated with the fast solar wind, but some of those such as the hole boundaries can be the VSSW sources if the flux expansion factors are sufficiently large. It should be noted that more VSSW sources are formed at 15–90° in the period between 2011 and 2015 (around the Cycle 24 maximum) than between 2001 and 2007 (the Cycle 23 declining phase). The averaged percentages for 15–90° are 54% and 76% for 2001–2007 and 2011–2015, respectively. Similar features are discernible in the data of the low-ΔN_e VSSW, although the percentage of low-latitude sources (0–15°) is smaller than that for all VSSW: 21% of the low-ΔN_e VSSW versus 29% for all VSSW on average. The majority of the low-ΔN_e VSSW sources are located at 15–90°. High-latitude (50–90°) sources of the low-ΔN_e VSSW develop at around the Cycle 23/24 minimum more extensively than for the case
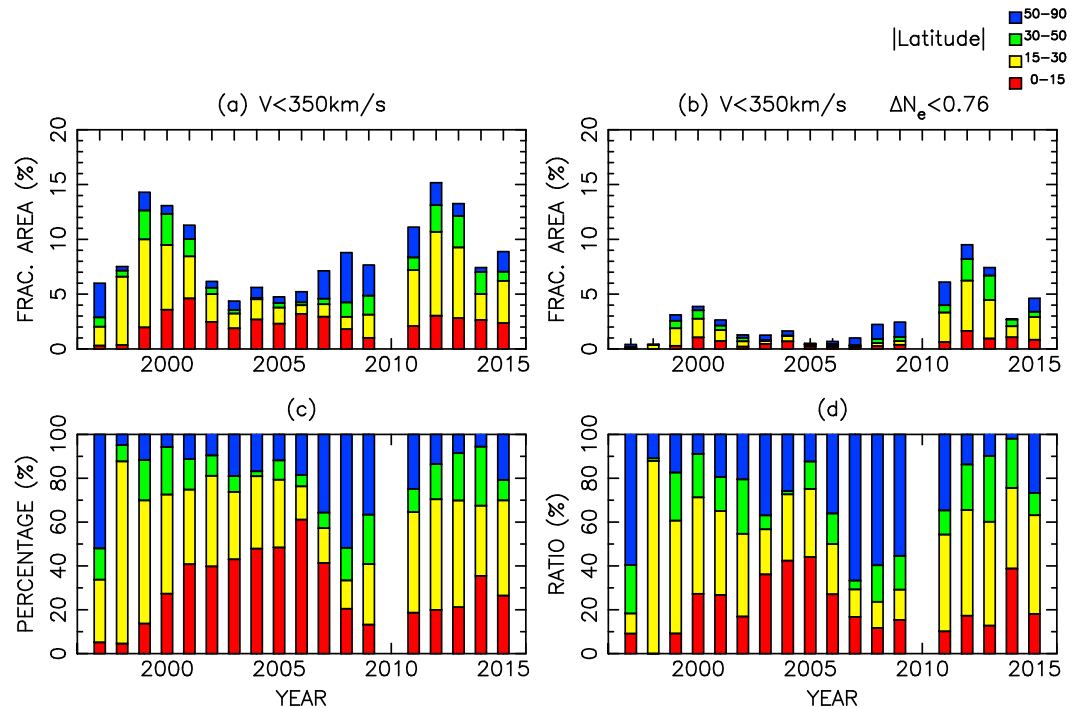
Figure 9. Annual variations of (a, b) fractional areas of very slow solar wind (VSSW) and (c, d) percentages of VSSW areas corresponding to four ranges of the source latitude on the photosphere: (red) 0–15°, (yellow) 15–30°, (green) 30–50°, and (blue) 50–90°. Plots (a) and (c) are data of all VSSW, and plots (b) and (d) are data of low-ΔN_e VSSW.

of all VSSW. The low-ΔN_e VSSW sources at 0–15° decrease from 23% in Cycle 23 to 18% in Cycle 24. However, any marked long-term trend like the one shown is Figure 3 is not observed for the source latitude distribution of the low-ΔN_e VSSW.

5.2. Flux Expansion Factors and Photospheric Field Strength

Figure 10a displays the variation in the yearly means of f for the (blue) low-ΔN_e VSSW ($V < 350$ km/s and $\Delta N_e < 0.76$), (red) high-ΔN_e VSSW ($V < 350$ km/s and $\Delta N_e > 0.76$), and (dashed line) $V > 350$ km/s during 1997–2015. Vertical bars on the data points denote the rms deviation in the yearly mean. As shown here, the yearly means of f for all VSSW data (including both the low- and high-ΔN_e VSSW) are higher than those for $V > 350$ km/s except for low-ΔN_e VSSW data in 2001, 2003, and 2013. This fact is generally consistent with the well-known inverse relation between the speed and the expansion factor (Hakamada & Kojima, 1999; Wang & Sheeley, 1990). Here it should be noted that the values of f for the high-ΔN_e VSSW are roughly constant during the analysis period. This fact suggests that f acts as a robust parameter to determine the solar wind speed (Fujiki et al., 2015; Tokumaru et al., 2017). Another important feature revealed here is that the yearly means of f for the low-ΔN_e VSSW are systematically smaller than those for the high-ΔN_e VSSW. Those during 2001–2003 are nearly the same as those for $V > 350$ km/s. Figure 10b shows the annual variation in the ratios of f for the low-ΔN_e VSSW to those for the high-ΔN_e VSSW. The ratios are less than 1, except for 3 years: 1998, 2005, and 2006, and they are as low as ∼0.5 for the period 1999–2004. The ratios tend to rise toward 1 after 2006, but they are still below 1. The average of the yearly ratio data is 0.77 ± 0.24. The years 1998, 2005, and 2006 correspond to the period when the occurrence of the low-ΔN_e VSSW is minimal. Therefore, the data of those years are likely to be affected by the small number of samples. The occurrence of the low-ΔN_e VSSW is also minimal in 1997. If we omit data for these years, we obtain 0.69 ± 0.19.

Figure 11a shows the variations in the yearly mean $|B_P|$ for the (blue) low-ΔN_e VSSW ($V < 350$ km/s and $\Delta N_e < 0.76$), (red) high-ΔN_e VSSW ($V < 350$ km/s and $\Delta N_e > 0.76$), and (dashed line) $V > 350$ km/s during 1997–2015. The yearly means of $|B_P|$ for the high-ΔN_e VSSW are larger than those for $V > 350$ km/s except for the period 2007–2009. Unlike f data, $|B_P|$ data exhibit a marked dependence on the solar cycle. This fact reflects the solar cycle variation of the photospheric fields. The low-ΔN_e VSSW tends to be associated with weaker $|B_P|$ than
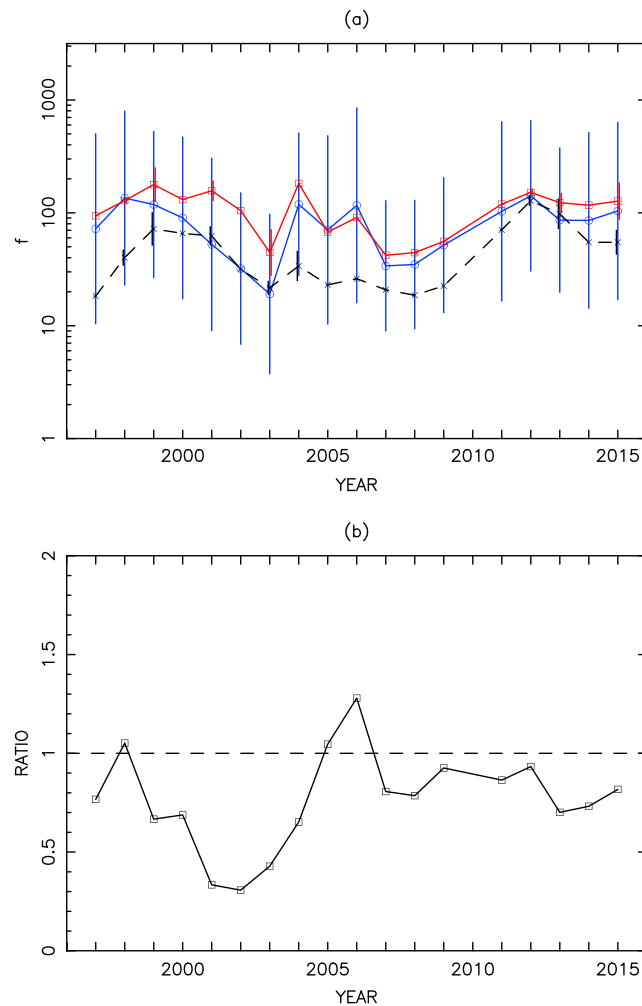
Figure 10. Annual variations of (a) expansion factors f for (red) high-ΔN_e very slow solar wind (VSSW) ($V < 350$ km/s and $\Delta N_e > 0.76$) and (blue) low-ΔN_e VSSW ($V < 350$ km/s and $\Delta N_e < 0.76$), (dashed line) $V > 350$ km/s. Vertical bars on the data are the root-mean-square deviations in the mean. The root-mean-square deviations are calculated after taking the log of the data. (b) Ratios of low-ΔN_e VSSW expansion factors to high-ΔN_e VSSW data.

high-ΔN_e VSSW. The mean fields of the low-ΔN_e VSSW do not appear to differ significantly from those in the solar wind with $V > 350$ km/s. The ratios of the mean $|B_P|$ of the low-ΔN_e VSSW to those of the high-ΔN_e VSSW are plotted in Figure 11b. The ratios are less than 1 for the period between 1997 and 2004, but they become larger than or nearly equal to 1 during 2005–2009. The ratios drop again below 1 after 2011 except for 2014. As a whole, the overall average of the ratios is slightly below 1, while its drop is within the rms deviation: 0.82 ± 0.24. There is a possibility that the data for 2005 and 2006 are affected by the insufficient statistics, but even if data for 2005 and 2006 are omitted, the drop is still within the rms deviation; the average ratio is 0.79 ± 0.22. Therefore, we cannot safely say that the difference in $|B_P|$ is statistically significant.

6. Discussion

The present study reveals that a significant reduction in the density of the VSSW occurs in Cycle 24. The VSSW in Cycle 23 was associated with a dense plasma, and this fact is consistent with in situ observations made by Helios in Cycle 21, that is, 1975–1985 (Sanchez-Diaz et al., 2016). However, this is no longer the case for Cycle 24; that is, the VSSW in this cycle becomes as rarefied as the fast wind, and hence, it cannot be regarded as a continuation of the normal slow wind. The significant reduction in the solar wind density in this cycle has already been reported from many earlier studies using in situ measurements (Jian et al., 2011; McComas et al., 2008, 2013; Tokumaru et al., 2012). A long-term declining trend in the solar wind density turbulence
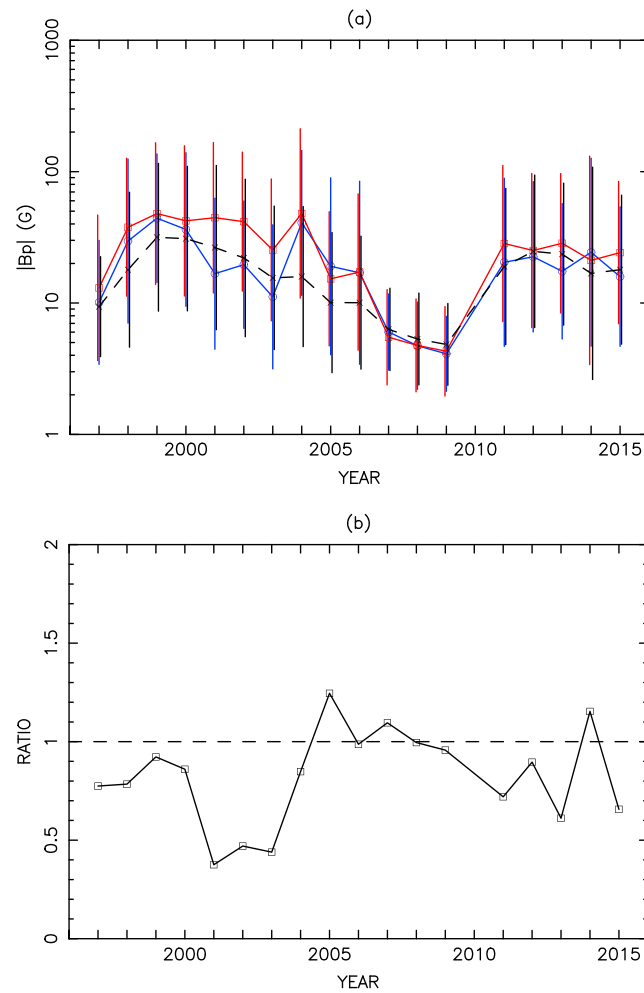
Figure 11. The same as Figure 10 but for photospheric fields $|B_P|$.

level during Cycles 23–24 has also been found from the analysis of ISEE IPS observations (Bisoi et al., 2014; Janardhan et al., 2011, 2015; Tokumaru et al., 2012), and this fact supports the rarefaction of the solar wind in this cycle. It should be noted here that the rarefaction of the solar wind is most remarkable for the speed range of the slow wind, though it takes place for all speed ranges (see Figure 13 of Tokumaru et al., 2012). This fact is consistent with the drastic change in the VSSW revealed from the present study.

We examine whether the inverse relation between V and ΔN_e is still valid for $V > 350$ km/s, even when the rarefaction of the solar wind occurs in Cycle 24 for all speed ranges. If the inverse relation were seriously affected by the rarefaction of the slow solar wind with $V > 350$ km/s, flattening of the power law indices or slopes would be observed. Figure 12 displays the best fit (a) power law indices and (b) slopes determined for the V-ΔN_e plot on a yearly basis. The power law indices and slopes were derived by fitting a function of $\Delta N_e = AV^B$ and $\Delta N_e = a+bV$, respectively, to IPS data for $V > 350$ km/s. The mean values for the indices and the slopes are indicated in the figure by horizontal dash-dotted lines: $B = -0.32 \pm 0.15$ and $b = -0.50 \pm 0.23$. A similar feature is observed in both plots. These results are basically the same as those presented the previous study in which IPS observations during 1997–2009 were analyzed: $B = -0.36 \pm 0.14$ and $b = -0.56 \pm 0.22$ (Tokumaru et al., 2012). Furthermore, no clear tendency toward a flatter value is found in the distribution of the data around the mean value except for those at solar maxima. Large excursions observed at or near solar maxima, that is, 2000 in Cycle 23, and 2012 and 2013 in Cycle 24, are mainly attributed to the effect of the rapid structural evolution of the solar wind. The distribution of the solar wind retrieved from the tomographic analysis of IPS observations is known to be blurred significantly by the rapid structural evolution at the solar maximum (Kojima et al., 2004).
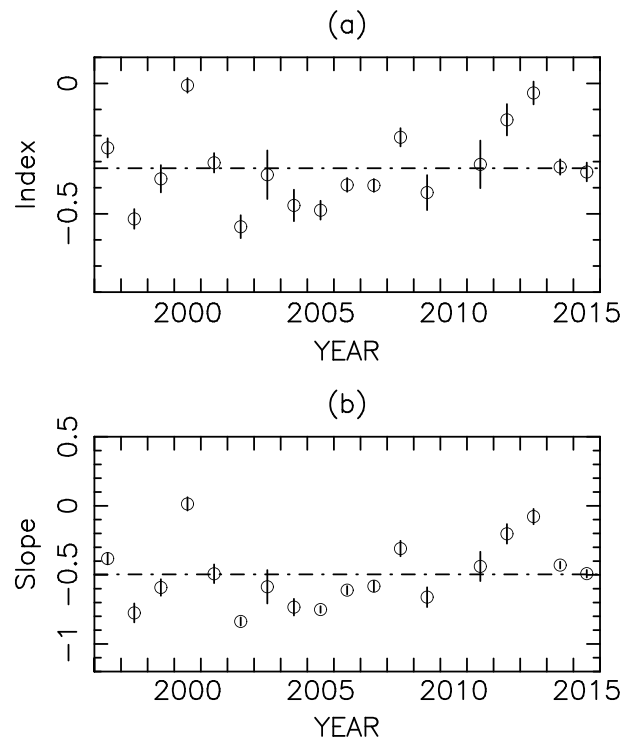
Figure 12. Time variations of the best fit (a) power law B indices and (b) slopes b. The functions $\Delta N_e = AV^B$ and $\Delta N_e = a + bV$ are fit to obtain these parameters. Horizontal dash-dotted lines in each plot show the average value, and vertical bars show the estimation errors.

This effect obscures the inverse relation between V and ΔN_e in the IPS data, resulting in flat indices or slopes in the V-ΔN_e plot. If the data for 2000, 2012, and 2013 are excluded, we obtain a steeper index or slope: $B = -0.38 \pm 0.09$ and $b = -0.58 \pm 0.15$. Although the IPS data for 2002 show a large excursion, they are kept here, since there is observational evidence to suggest that they correspond to the declining phase of Cycle 23, for example, reduced sunspot number and reappearance of the polar fast solar wind. Therefore, as long as we examine IPS observations up to 2015, rarefaction of the slow solar wind in this cycle does not appear to affect the overall feature of the inverse relation between V and ΔN_e for $V > 350$ km/s.

The rarefaction of the VSSW is thought to influence the interaction between the slow and fast winds at the stream interface. The fast wind is decelerated during propagation in the heliosphere through the interaction with the slow wind. This effect depends on the speed difference between the fast and slow winds, and a severe interaction is expected to occur at the stream interface between the VSSW and the fast wind, as demonstrated via the 1-D magnetohydrodynamic model calculations (Sanchez-Diaz et al., 2016). The effect of the stream-stream interaction also depends on the density of the slow wind. The rarefaction of the slow wind weakens the stream-stream interaction and causes the fast wind to propagate over large distances, being less decelerated than the case of a nonrarefied slow wind. This means retarded growth of the interaction region, which leads to the modification of its 3-D structure in the heliosphere. Since the pronounced rarefaction predominantly occurs only for the VSSW in Cycle 24, as revealed by the present study, its impact to the global heliosphere is limited. If the density of the slow wind with $V > 350$ km/s reduces remarkably so as to change the overall feature of the V-ΔNe relation in future, it will impose a significant impact on the 3-D structure of the interaction region in the heliosphere.

The present study shows that the sources of the low-ΔN_e VSSW are located at middle or high latitudes (15–90°) on the photosphere more often than those of all VSSW. The low-ΔN_e VSSW is found to be associated with systematically smaller expansion factors and weaker photospheric fields than the high-ΔN_e VSSW, although the difference in the field is statistically insignificant. These facts suggest that the low-ΔN_e VSSW sources are located in the quiet Sun region, not in the vicinity of the active region. We consider that the source of the low-ΔN_e VSSW may be closely associated with pseudostreamers, which separate coronal holes of the same polarity (Wang et al., 2007) and also which have recently been regarded as a possible additional source

of the slow wind (Owens et al., 2014; Riley & Luhmann, 2012). Pseudostreamers are usually associated with very small expansion factors (Riley & Luhmann, 2012). The occurrence of pseudostreamers shows a solar cycle variation; their occurrence drops to a minimum at solar minima and increases at solar maxima, overwhelming the occurrence of dipolar streamers (Owens et al., 2014). The latitude extent of pseudostreamers also shows a solar cycle variation, similar to that of dipolar streamers, but with a more rapid growth and decline, and thus, pseudostreamers tend to be observed at higher latitudes than dipolar streamers for the period around the solar maximum (Owens et al., 2014). These features of pseudostreamers are consistent with the properties of the low-ΔN_e VSSW revealed by the present study. A detailed analysis of the relation between the low-ΔN_e VSSW and pseudostreamers is an interesting subject, though it is beyond the scope of this paper.

The current solar cycle is characterized by weak solar dynamo activity, which is at a 100 year low, and some peculiar aspects of the solar wind have been reported from recent studies, for example, increased (decreased) occurrence of low-latitude (polar) fast winds in the Cycle 23/24 minimum (Tokumaru et al., 2009, 2010) and enhanced north-south asymmetry in the global distribution of the solar wind (Tokumaru et al., 2015). These are considered as interplanetary consequences of a peculiarity in the Sun's magnetic field of this cycle. The rarefaction of the solar wind in Cycle 24 is also considered to be one of manifestations of the weak solar dynamo activity. A linear relationship was found between the proton density and the radial interplanetary magnetic field component B_r in the fast solar wind and also between B_r and the polar photospheric LOS field (Riley et al., 2010). On the basis of numerical simulations, this fact was ascribed to the reduced coronal heating rate in this cycle. A similar linear relationship was revealed between the solar wind mass flux and the normalized radial interplanetary magnetic field component multiplied by the correction factor (Zhao & Fisk, 2011). This result was interpreted by a solar wind acceleration model in which reconnection of closed loops with open-field lines in the photosphere was assumed (Fisk, 2003). Furthermore, it was found from an analysis of in situ measurements at 1 AU that the mass flux at the coronal base increases almost linearly with the footpoint field strength (Wang & Sheeley Jr, 2013). The results obtained from the present study clearly demonstrate that remarkable rarefaction occurs selectively for the very low speed wind. This fact may have important implications for the physical processes of solar wind acceleration and coronal heating. The results obtained here may also provide an insight into the solar wind condition during the grand minimum, when the solar dynamo activity greatly drops over many cycles. A recent analysis of sunspot data suggests a further decline of solar activity in the future (Zachilas & Gkana, 2015). It is exceedingly interesting to elucidate the evolution of the solar wind in response to such a serious weakening of solar activity. If marked rarefaction of the solar wind occurs for a speed range much higher than 350 km/s, the influence on the 3-D structure of the heliosphere would be significant.

7. Summary

ISEE IPS observations during 1997–2015, that is, Cycle 23–24, were analyzed to investigate the properties of the VSSW (with $V < 350$ km/s) and its long-term variation. It is found that the VSSW evolves drastically during the analysis period. The fractional areas of the VSSW are found to show a distinct solar cycle dependence: they increase with solar activity, peaking at solar maxima. More importantly, it is demonstrated that the VSSW observed in Cycle 23 was mostly associated with high ΔN_e (>1), but that observed in Cycle 24 was dominated by low ΔN_e (< 0.76). This fact suggests that the VSSW, which was formerly associated with a dense plasma, has been rarefied significantly in this cycle. The tendency for rarefaction is also found for the fast wind but much less prominently than for the VSSW. A clear piece of evidence that supports the rarefaction of the VSSW is obtained from in situ measurements at 1 AU during 1998–2015. The latitude of the VSSW source shows solar cycle variation: the low-latitude (0–15°) sources increase in the declining phase of Cycle 23 and at the Cycle 24 maximum, whereas middle- and high-latitude sources increase in the periods near the solar minimum. The low-ΔN_e VSSW sources tend to be located at middle or high latitudes more frequently than all VSSW. The magnetic field properties of the VSSW source were investigated from an analysis using the PFSS model. The result indicates that the low-ΔN_e VSSW is associated with a smaller expansion factor than the high-ΔN_e VSSW. We also find that the low-ΔN_e VSSW is associated with a weaker photospheric field than the high-ΔN_e VSSW, but this difference is within the rms deviation in the mean. Therefore, further study is needed to arrive at a conclusion. The results obtained here may suggest that the low-ΔN_e VSSW source is located in the quiet Sun region and that more open-field regions, which produce the VSSW, are formed in this cycle than in the previous cycle as a consequence of the weakening of the Sun's magnetic field.

References

Asai, K., Kojima, M., Tokumaru, M., Yokobe, A., Jackson, B. V., Hick, P. L., & Manoharan, P. K. (1998). Heliospheric tomography using interplanetary scintillation observations: 3. Correlation between speed electron density fluctuations in the solar wind. *Journal of Geophysical Research*, *103*, 1991–2001. https://doi.org/10.1029/97JA02750

Bisoi, S. K., Janardhan, P., Ingale, M., Subramanian, P., Ananthakrishnan, S., Tokumaru, M., & Fujiki, K. (2014). A study of density modulation index in the inner solar wind during solar cycle 23. *The Astrophysical Journal*, *795*, 69. https://doi.org/10.1088/0004-637X/795/1/69

Coles, W. A., Harmon, J. K., Lazarus, A. J., & Sullivan, J. D. (1978). Comparison of 74-MHz interplanetary scintillation and IMP 7 observations of the solar wind during 1973. *Journal of Geophysical Research*, *83*, 3337–3341. https://doi.org/10.1029/JA083iA07p03337

Fisk, L. A. (2003). Acceleration of the solar wind as a result of the reconnection of open magnetic flux with coronal loops. *Journal of Geophysical Research*, *108*, 1157. https://doi.org/10.1029/2002JA009284

Fujiki, K., Kojima, M., Tokumaru, M., Ohmi, T., Yokobe, A., Hayashi, K., et al. (2003). How did the solar wind structure change around the solar maximum? From interplanetary scintillation observation. *Annales de Geophysique*, *21*, 1257–1261. https://doi.org/10.5194/angeo-21-1257-2003

Fujiki, K., Tokumaru, M., Iju, T., Hakamada, K., & Kojima, M. (2015). Relationship between solar-wind speed and coronal magnetic field properties. *Solar Physics*, *290*, 2491–2505. https://doi.org/10.1007/s11207-015-0742-8

Hakamada, K., & Kojima, M. (1999). Solar wind speed and expansion rate of the coronal magnetic field during Carrington rotation 1909. *Solar Physics*, *187*, 115–122. https://doi.org/10.1023/A:1005183914772

Janardhan, P., Bisoi, S. K., Ananthakrishnan, S., Tokumaru, M., & Fujiki, K. (2011). The prelude to the deep minimum between solar cycles 23 and 24: Interplanetary scintillation signatures in the inner heliosphere. *Geophysical Research Letters*, *38*, L20108. https://doi.org/10.1029/2011GL049227

Janardhan, P., Bisoi, S. K., Ananthakrishnan, S., Tokumaru, M., Fujiki, K., Jose, L., & Sridharan, R. (2015). A 20 year decline in solar photospheric magnetic fields: Inner-heliosphere signatures and possible implications. *Journal of Geophysical Research: Space Physics*, *120*, 5306–5317. https://doi.org/10.1002/2015JA021123

Jian, L. K., Russell, C. T., & Luhmann, J. G. (2011). Comparing solar minimum 23/24 with historical solar wind records at 1 AU. *Solar Physics*, *274*, 321–344. https://doi.org/10. 1007s11207-011-9737-2

Kojima, M., Fujiki, K., Hirano, M., Tokumaru, M., Ohmi, T., & Hakamada, K. (2004). Solar wind properties from IPS observations. In G. Poletto & S. T. Suess (Eds.), *The Sun and the heliosphere as an integrated system, Astrophysics and Space Science Library* (Vol. 317, pp. 147–178). Dordrecht: Springer. https://doi.org/10.1007/978-1-4020-2831-1_6

Kojima, M., Fujiki, K., Ohmi, T., Tokumaru, M., Yokobe, A., & Hakamada, K. (1999). Low-speed solar wind from the vicinity of solar active region. *Journal of Geophysical Research*, *104*, 16,993–17,003. https://doi.org/10.1029/1999JA900177

Kojima, M., & Kakinuma, T. (1990). Solar cycle dependence of global distribution of the solar wind speed. *Space Science Reviews*, *53*, 173–222. https://doi.org/10.1007/BF00212754

Kojima, M., Tokumaru, M., Fujiki, K., Hayashi, K., & Jackson, B. V. (2007). IPS tomographic observations of 3D solar wind structure. *Astronomical and Astrophysical Transactions*, *26*, 467–476. https://doi.org/1080/105567990701596200

Kojima, M., Tokumaru, M., Watanabe, H., Yokobe, A., Asai, K., Jackson, B. V., & Hick, P. L. (1998). Heliospheric tomography using interplanetary scintillation observations: 2. Latitude and heliocentric distance dependence of solar wind structure at 0.1-1 AU. *Journal of Geophysical Research*, *103*(A2), 1981–1989. https://doi.org/10.1029/97JA02162

Le Chat, G., Issautier, K., & Meyer-Vernet, N. (2012). The solar wind energy flux. *Solar Physics*, *279*, 197–205. https://doi.org/10.1007/s11207-012-9967-y

McComas, D. J., Angold, N., Elliott, H. A., Livadiotis, G., Schwadron, N. A., Skoug, R. M., & Smith, C. W. (2013). Weakest solar wind of the space age and the current "mini" solar maximum. *The Astrophysical Journal*, *779*, 2. https://doi.org/10.1088/0004-637X/779/1/2

McComas, D. J., Bame, S. J., Barker, P., Feldman, W. C., Phillips, J. L., Riley, P., & Griffee, J. W. (1998). Solar Wind Electron Proton Alpha Monitor (SWEPAM) for the Advanced Composition Explorer. *Space Science Reviews*, *86*, 563–612. https://doi.org/10.1023/A:1005040232597

McComas, D. J., Ebert, R. W., Elliott, H. A., Goldstein, B. E., Gosling, J. T., Schwadron, N. A., & Skoug, R. M. (2008). Weaker solar wind from the polar coronal holes and the whole Sun. *Geophysical Research Letters*, *35*, L18103. https://doi.org/10.129/2008GL034896

Mullan, D. J. (1983). Momentum flux invariance in the solar wind. *The Astrophysical Journal*, *272*, 325–328. https://doi.org/10.1007/BF00148287

Neugebauer, M. (1992). Knowledge of coronal heating and solar-wind acceleration obtained from observations of the solar wind near 1 AU. In E. Marsch & R. Schwenn (Eds.), *Solar wind seven, proceedings of the third COSPAR Colloquium Held in Goslar, Germany, 16–20 September 1991* (pp. 69–78). Oxford: Pergamon Press.

Ohmi, T., Kojima, M., Tokumaru, M., Fujiki, K., & Hakamada, K. (2004). Origin of the slow solar wind. *Advances in Space Research*, *33*, 689–695. https://doi.org/10.1016S0273-1177(03)00238-2

Owens, M. J., Crooker, N. U., & Lockwood, M. (2014). Solar cycle evolution of dipolar and pseudostreamer belts and their relation to the slow solar wind. *Journal of Geophysical Research: Space Physics*, *119*, 36–46. https://doi.org/10.1002/2013JA019412

Phillips, J. L., Bame, S. J., Barnes, A., Barraclough, B. L., Feldman, W. C., Goldstein, B. E., et al. (1995). Ulysses solar wind plasma observations from pole to pole. *Geophysical Research Letters*, *33*, 3301–3304. https://doi.org/10.1029/95GL03094

Richardson, J., & Wang, C. (1999). The global nature of solar cycle variations of the solar wind dynamic pressure. *Geophysical Research Letters*, *26*, 561–564. https://doi.org/10.1029/1999GL900052

Riley, P., & Luhmann, J. G. (2012). Interplanetary signatures of unipolar streamers and the origin of the slow solar wind. *Solar Physics*, *277*, 355–373. https://doi.org/10.1007/s11207-011-9909-0

Riley, P., Mikic, Z., Lionello, R., Linker, J. A., Schwadron, N. A., & McComas, D. J. (2010). On the relationship between coronal heating, magnetic flux, and the density of the solar wind. *Journal of Geophysical Research*, *115*, A06104. https://doi.org/10.1029/2009JA015131

Russell, C. T., Luhmann, J. G., & Strangeway, R. J. (2016). The solar wind and heliosphere. *Space Physics Chapter*, *5*, 145–198.

Sanchez-Diaz, E., Rouillard, A. P., Lavraud, B., Segura, K., Tao, C., Pinto, R., et al. (2016). The very slow solar wind: Properties, origin and variability. *Journal of Geophysical Research: Space Physics*, *121*, 2830–2841. https://doi.org/10.1002/2016JA022433

Steinitz, R., & Eyni, M. (1980). Global properties of the solar wind. I—The invariance of the momentum flux density. *The Astrophysical Journal*, *241*, 417–424. https://doi.org/10.1086/158355

Tokumaru, M. (2013). Three-dimensional exploration of the solar wind using observations of interplanetary scintillation. *Proceedings of the Japan Academy, Series B*, *89*, 67–79. https://doi.org/10.2183/pjab.89.67

Tokumaru, M., Fujiki, K., & Iju, T. (2015). North-south asymmetry in global distribution of the solar wind speed during 1985–2013. *Journal of Geophysical Research: Space Physics*, *120*, 3283–3296. https://doi.org/10.1002/2014JA020765

Tokumaru, M., Kojima, M., & Fujiki, K. (2010). Solar cycle evolution of the solar speed distribution from 1985 to 2008. *Journal of Geophysical Research*, *115*, A04102. https://doi.org/10.1029/2009JA014628

Tokumaru, M., Kojima, M., & Fujiki, K. (2012). Long-term evolution in the global distribution of solar wind speed and density fluctuations during 1997–2009. *Journal of Geophysical Research*, *117*, A06108. https://doi.org/10.1029/2011JA017379

Tokumaru, M., Kojima, M., Fujiki, K., & Hayashi, K. (2009). Non-dipolar solar wind structure observed in the cycle 23/24 minimum. *Geophysical Research Letters*, *36*, L09101. https://doi.org/10.1029/2009GL037461

Tokumaru, M., Satonaka, D., Fujiki, K., Hayashi, K., & Hakamada, K. (2017). Relation between coronal hole areas and solar wind speeds derived from interplanetary scintillation measurements. *Solar Physics*, *292*, 41. https://doi.org/10.1007/s11207-017-1066-7

Tokumaru, M. M., Kojima, M., Ishida, Y., Yokobe, A., & Ohmi, T. (2000). Large-scale structure of solar wind turbulence near solar activity minimum. *Advances in Space Research*, *25*, 1943–1946. https://doi.org/10.1016/S0273-1177(99)00630-4

Wang, Y.-M., & Sheeley, N. R. Jr. (1990). Solar wind speed and coronal flux tube expansion. *The Astrophysical Journal*, *355*, 726–732. https://doi.org/10.1086/168805

Wang, Y.-M., & Sheeley, N. R. Jr. (2013). Solar wind and interplanetary field during very low amplitude sunspot cycles. *The Astrophysical Journal*, *764*, 90. https://doi.org/10.1088/0004-637X/764/1/90

Wang, Y.-M., Sheeley, N. R. Jr., & Rich, N. B. (2007). Coronal pseudostreamers. *The Astrophysical Journal*, *658*, 1340–1348. https://doi.org/10.1086/511416

Zachilas, L., & Gkana, A. (2015). On the verge of a grand solar minimum: A second Maunder minimum? *Solar Physics*, *290*, 1457–1477. https://doi.org/10.1007/s11207-015-0684-1

Zhao, L., & Fisk, L. (2011). Understanding the behavior of the heliospheric magnetic field and the solar wind during the unusual solar minimum between Cycles 23 and 24. *Solar Physics*, *274*, 379–397. https://doi.org/10.1007/s11207-011-9840-4